Article

Hydration Effects on the Stability of Calcium Carbonate Pre-Nucleation Species

Alejandro Burgos-Cara [1] iD **, Christine V. Putnis** [2,3] **, Carlos Rodriguez-Navarro** [1] iD **and Encarnacion Ruiz-Agudo** [1,*]

[1] Mineralogy and Petrology Department, University of Granada, 18071 Granada, Spain; aburgoscara@ugr.es (A.B.-C.); carlosrn@ugr.es (C.R.-N.)
[2] Institut für Mineralogie, University of Münster, 48149 Münster, Germany; putnisc@uni-muenster.de
[3] Department of Chemistry, Curtin University, Perth 6845, Australia
[*] Correspondence: encaruiz@ugr.es; Tel.: +34-958-240-473

Abstract: Recent experimental evidence and computer modeling have shown that the crystallization of a range of minerals does not necessarily follow classical models and theories. In several systems, liquid precursors, stable pre-nucleation clusters and amorphous phases precede the nucleation and growth of stable mineral phases. However, little is known on the effect of background ionic species on the formation and stability of pre-nucleation species formed in aqueous solutions. Here, we present a systematic study on the effect of a range of background ions on the crystallization of solid phases in the $CaCO_3$-H_2O system, which has been thoroughly studied due to its technical and mineralogical importance, and is known to undergo non-classical crystallization pathways. The induction time for the onset of calcium carbonate nucleation and effective critical supersaturation are systematically higher in the presence of background ions with decreasing ionic radii. We propose that the stabilization of water molecules in the pre-nucleation clusters by background ions can explain these results. The stabilization of solvation water hinders cluster dehydration, which is an essential step for precipitation. This hypothesis is corroborated by the observed correlation between parameters such as the macroscopic equilibrium constant for the formation of calcium/carbonate ion associates, the induction time, and the ionic radius of the background ions in the solution. Overall, these results provide new evidence supporting the hypothesis that pre-nucleation cluster dehydration is the rate-controlling step for calcium carbonate precipitation.

Keywords: background electrolytes; dehydration kinetics; calcium carbonate; calcite; clusters; nucleation; vaterite; ACC

1. Introduction

Calcium carbonate precipitation has been widely studied due to the extensive distribution of carbonates, predominantly calcium carbonate, in surface rocks of the earth and scale formation in industrial processes. It presents a relatively simple model system to work with, and its wide occurrence in many biominerals provides interdisciplinary significance [1,2]. It is known that many organic additives play a key role in nucleation and growth processes, with either enhancing or hindering effects [3–8]. The latter frequently leads to the stabilization of more soluble metastable phases, such as amorphous phases (i.e., amorphous calcium carbonate, or ACC), that are known to play a key role in biomineralization processes [9–12]. However, not only organic molecules have been recognized to either modify crystal morphology or stabilize more soluble precursor phases. Other ions present in solution, such as Mg^{2+}, may also influence mineral formation processes [13–17]. The role that background ions play in calcium carbonate precipitation, either from experimental reagents, or additionally dosed or naturally present in aqueous environments, has been frequently neglected or

underestimated. Recent experimental and computational results [18,19] suggest that Ca^{2+} and $CO_3{}^{2-}$ ions can associate into stable complexes prior to the onset of liquid or solid $CaCO_3$ formation and that, when conditions are favorable, this process of solute clustering is primarily controlled by the release of water molecules from ion hydration layers [20]. Therefore, any factor affecting cluster solvation should influence the stability of pre-nucleation ion associates, and thus also affect nucleation.

Background electrolytes can affect nucleation kinetics, crystal growth, dissolution, crystal size distribution, and the purity of precipitates by inducing changes in the aqueous solvation environment [21–25]. Ions in solution are able to modify water structure dynamics in their local environment as a result of effects associated with their hydration shells [26], which immobilize and electrostrict water [27]. The dehydration kinetics of ions (or clusters) in solution will be a competition between ion (or clusters)-water and water-water interactions [28,29], which can be significantly modified by the presence of background ions in solution [30]. At low ionic strength, the effect of background electrolytes on ion (or clusters)-water electrostatic interactions will be dominant [26].

We present a systematic study on the effect of a series of 1:1 background electrolytes on the precipitation of calcium carbonate. Experiments were performed under conditions of low ionic strength. Our main goal was to test the basic hypotheses that (i) the effect of electrolytes on the stability of pre-nucleation species and the onset of nucleation can be related to the influence of background electrolytes on the solvation of the ions building the crystals; and (ii) the systematic trends observed in the stability of pre-nucleation species and the onset of nucleation for the different background salts are due to the intrinsic properties of the background ions. To do so, we performed $CaCO_3$ precipitation (titration) experiments in the presence of different background electrolytes and at different ionic strengths, continuously monitoring pH, free-Ca^{2+} concentration, conductivity, and solution transmittance in batch reactors. At the same time, we studied the particle size distribution and the structural and textural features of precipitated phases.

2. Materials and Methods

2.1. Titration Experiments

Two types of experiments were performed in order to study the influence of different background electrolytes on calcium carbonate precipitation. In both types of experiments, a 10 mM aqueous calcium solution was continuously added, at a rate of 2 µL/s, into a reactor containing 100 mL of a 10 mM carbonate solution. The first type of experiment (Type I) was performed by changing the counter-ion of the salts used for calcium carbonate precipitation. For this purpose, Li_2CO_3, Na_2CO_3, K_2CO_3 and Cs_2CO_3 were used as carbonate sources, and $CaCl_2$, $CaBr_2$ and CaI_2 were used as calcium sources. This allowed us to study the influence of different background ions (both anions and cations) at a very low ionic strength (IS) of 0.026, defined according to Equation (1).

$$IS = \frac{1}{2} \sum_{i=1}^{n} c_i \cdot z_i^2 \tag{1}$$

where c_i is the molar concentration of "i" ion and z_i the charge of each ion.

The second type of experiment (Type II) was performed by selecting Na_2CO_3 and $CaCl_2$ as the carbonate and calcium sources, respectively, for calcium carbonate precipitation. Different background ions were introduced as foreign salts, in addition to the NaCl already present in the growth solution (i.e., LiCl, NaCl, NaBr, NaI, KCl and CsCl) at two different concentrations, 10 and 25 mM, with the aim to study both the effect of the background ions themselves, and the influence of two different ionic strengths (i.e., IS = 0.035 and 0.049, respectively).

Both types of experiments were performed using a 200 mL jacketed glass reactor coupled to a thermostatic bath, in order to maintain a constant T of 25 °C inside the reactor, which included a stirrer module (module 801, Metrohm, Gallen, Switzerland). The pH was measured using a glass electrode from Metrohm, conductivity with an 856 conductivity module (Metrohm, Gallen, Switzerland),

transmittance with an Optrode sensor (Metrohm, Gallen, Switzerland) using a wavelength of 610 nm, and free calcium in solution (Ca^{2+}) with an ion-selective electrode (ISE, Mettler-Toledo, DX240-Ca, Columbus, OH, USA), using the pH electrode as a reference electrode. Sensors and dosing devices were coupled to a Titrando 905 module from Metrohm controlled with the software Tiamo v2.5 (Metrohm, Gallen, Switzerland). The above parameters (pH, transmittance, conductivity, and free-Ca) were recorded continuously during precipitation experiments.

Inorganic salts used in the two types of experiments (Li_2CO_3, Na_2CO_3, K_2CO_3, Cs_2CO_3, $CaCl_2$, $CaBr_2$, CaI_2, LiCl, NaCl, NaBr, NaI, KCl and CsCl) were purchased from Sigma-Aldrich (Merck Darmstadt, Germany) with purity of at least 99%. Solutions used in titration experiments were prepared with ultrapure water Type I + (resistivity $\geq$ 18.2 MΩ·cm). The initial pH values inside the reactor for the different type of experiments and salts were 11.05 $\pm$ 0.05 (IS = 0.026, Type I), 10.93 $\pm$ 0.04 (IS = 0.035, Type II), and 10.91 $\pm$ 0.05 (IS = 0.049, Type II). pH adjustment was avoided in order not to introduce more foreign ions into solutions, which would also modify the ionic strength (IS). In any case, measured pH changes (i.e., reduction) over the course of the titration experiments never exceeded 0.1 pH units. Higher reactant concentrations were avoided because at low IS, changes in activity coefficients for the different background ions tested could be considered as negligible [31,32].

2.2. Dynamic Light Scattering

During titration experiments, the controlled reference heterodyne method and in situ dynamic light scattering (DLS) were used to evaluate the time evolution of the precipitate particle size distribution as it referred to equivalent sphere diameter. Measurements were conducted at a scattering angle of 180° using a Microtrac NANO-flex particle size analyzer (MTB, Madrid, Spain) equipped with a diode laser (λ = 780 nm, 5 mW) and a 1 m-long flexible measuring probe (diameter = 8 mm) with sapphire window as the sample interface. Scattering was continuously monitored in situ during titration experiments, with an acquisition time of 30 s per run during 120 consecutive runs. DLS measurements started immediately before the slope of free-Ca^{2+} begun to flatten during titration experiments. Particle size distributions (PSDs) were computed with the Microtrac FLEX application software package (v.11.1.0.2, Microtrac, Montgomeryville, PA, USA). The presented PSD graphs show average values of particle size for the 120 consecutive measurements. Background scattering for pure water, as well as for solutions of each individual salt tested were collected. However, no particles within the analyzed size range were detected in these control runs.

2.3. Electron Microscopy

An Auriga field emission-scanning electron microscope (FE-SEM, ZEISS, Jena, Germany) was used for morphology examinations of calcium carbonate precipitates formed both at the early stages of precipitation and at the end of titration experiments. Prior to observations, samples were carbon coated. Secondary electron (SE) images were acquired using a SE-InLens detector. Observations were carried out at an accelerating voltage of 3 kV.

## 2.4. X-ray Diffraction Analysis

Solid phases formed during the different precipitation tests were analyzed by X-ray diffraction (XRD, PANalytica, Eindhoven, The Netherlands) using a Panalytical X′Pert PRO diffractometer. The following working conditions were used: radiation CuKα (λ = 1.5405 Å), voltage 45 kV, current 40 mA, scanning angle (2θ) 10°–70° and goniometer speed 0.016° 2θ s^{-1}.

3. Results

3.1. Type I Experiments

#### 3.1.1. Effect of Different Counter-Ions in the Carbonate or Calcium Sources

Changing the cation (M^+) in the carbonate source led to appreciable changes in both the maximum free calcium concentration (Ca^{2+}_{max}) reached in titration experiments, and the corresponding induction time for the onset of precipitation (Figure 1). To correlate experimental values from titration experiments, the ionic radius was selected as the most simple and straightforward variable to fit our results. However, other parameters, such as the hydration enthalpy of an ion, could be used to obtain similar trends (see Figure S1). As depicted in Figure 1a,b, for the same calcium salt (i.e., $CaCl_2$), the lower the ionic radius of the cation (M^+) in the carbonate source (M_2CO_3), the higher the induction time and corresponding concentration of Ca^{2+}_{max} reached before the onset of spontaneous precipitation. In parallel, using Na_2CO_3 as the carbonate source, and a calcium source (CaX_2) with different anions (X^-), a slight decrease in Ca^{2+}_{max} concentration and induction time with increasing ionic radius of anions was observed (Figure 1c,d). Although differences between electrolytes are in some cases (e.g., K^+ and Cs^+) within errors, there is a clear observable trend in both the induction time and maximum free calcium concentration for the onset of nucleation, which in both cases (X^- and M^+) decreases with increasing ionic size. Nonetheless, it should be taken into account that the radius of a hydrated Cs^+ ion is slightly larger than K^+, whereas the hydrated radius of ions tends to decrease with increasing atomic number (i.e., $r + \Delta r$: $Li^+ > Na^+ > Cs^+ > K^+$). This suggests that the effective hydrated radius could be a relevant parameter to consider in the particular case of K^+ and Cs^+. On the other hand, a lower effect of the background electrolyte is observable in the case of anions. This appears to be related to the less structured solvation shell of anions (e.g., the hydration enthalpy of the anions is typically smaller than that of the cations, see Figure S1).
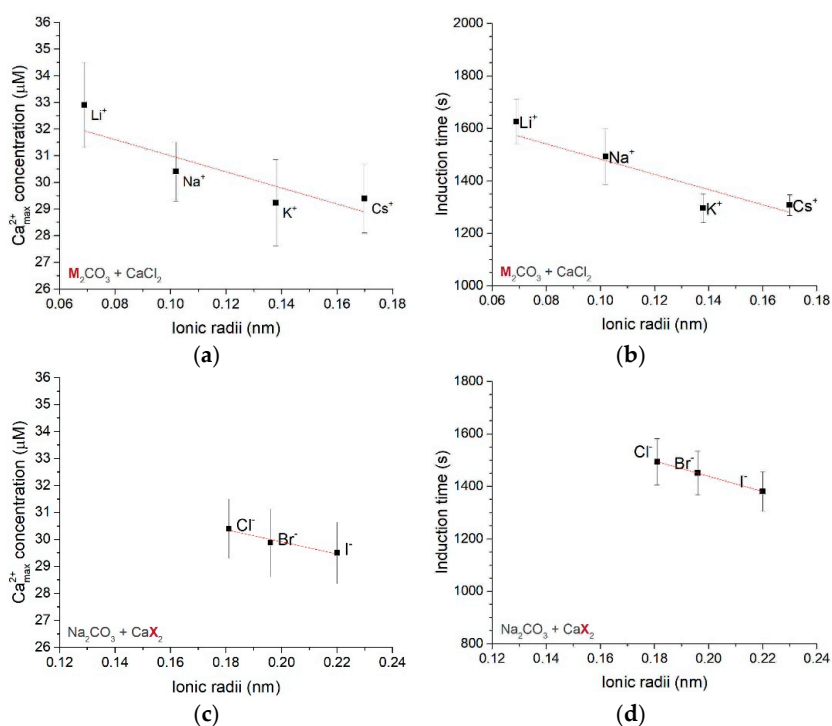
Figure 1. Maximum free Ca^{2+} concentration and corresponding induction time for type I titration experiments. (**a**,**b**) $CaCl_2$ was added to solutions of different carbonate sources (Li_2CO_3, Na_2CO_3, K_2CO_3, Cs_2CO_3) placed in the reactor. (**c**,**d**) Na_2CO_3 was always present in the reactor, and different calcium sources ($CaCl_2$, $CaBr_2$, CaI_2) were continuously added to the reactor. Errors bars show $2\sigma_N$.

3.1.2. Dynamics of Calcium Carbonate Binding

From titration experiments, the free Ca^{2+} concentration inside the reactor could be plotted vs. time (Figure 2a,b). Before precipitation, the amount of total calcium added to the reactor was always higher than the free calcium concentration measured by the ion-selective electrode. The latter is related to ion pairing and clustering phenomena in the pre-nucleation regime [20]. On the one hand, as depicted in Figure 2, larger background ions, both in the case of different background anions in the calcium source or cations in the carbonate source, seem to slightly increase the slope of the measured free calcium concentration. This indicates a lower ion pairing/clustering. On the other hand, in the case of Li_2CO_3 as the carbonate source, it was also observed that the Ca^{2+} concentration at the steady state (Figure 2a), corresponding to the solubility product of the precipitating phase (the more soluble one, if two or more phases form after the initial precipitated phase [20]), was higher compared to the other carbonate sources. The latter suggests a lower stability of the precipitating phase, as stated by Gebauer et al. [20]. In this case, it is likely that a more soluble ACC phase, possibly similar to the ACC II phase suggested by Gebauer et al. [20], was the first to precipitate in this system. Alternatively, the latter could be also explained by a different water content in the precipitating ACC, as suggested by Rodriguez-Navarro et al. [33] (i.e., a higher water content results in higher solubilities or size-related solubility effects; [34] see below). In contrast, it was systematically observed that when using CaI_2 as the calcium source, the free calcium concentration decreased linearly after precipitation (no actual steady state was observed), which suggested a faster transition, possibly by means of a dissolution–reprecipitation process, to produce a less soluble phase (Figure 2b).
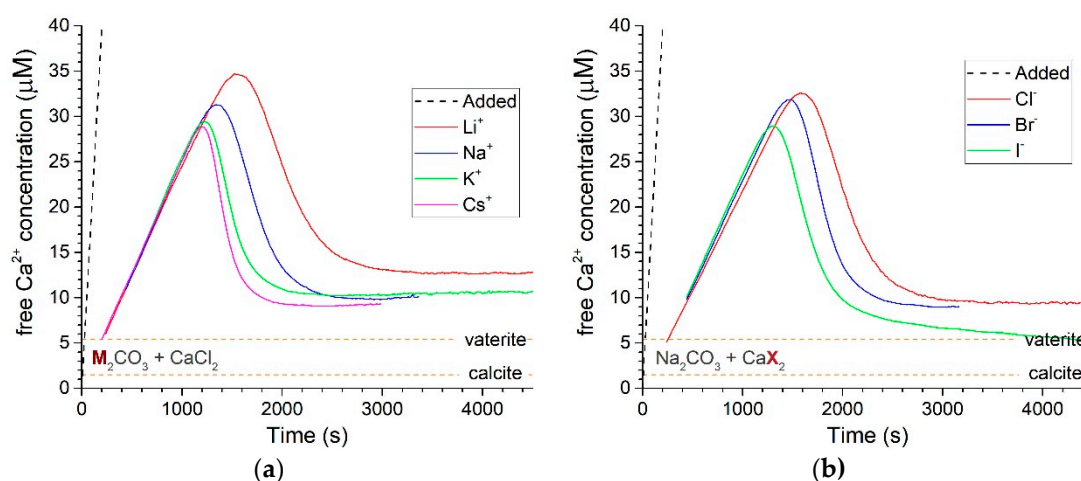

Figure 2. Free-Ca^{2+} concentration measured in type I titration experiments for (**a**) different background cations in the carbonate source and (**b**) different background anions in the calcium source. Horizontal orange dashed lines in (**a**,**b**) show the expected free-Ca^{2+} concentration for the different phases according to calculations using the geochemical computer code (PHREEQc) [35]. The nearly vertical black dashed line shows the time evolution of the total amount of calcium dosed during the titration experiment.

3.1.3. Free Energy of Ion Associates

The free energy of Ca^{2+} and CO_3^{2-} ions associated into stable complexes, present before the onset of $CaCO_3$ solid phase formation, could be calculated using the thermodynamic expression $\Delta G_{binding} = -RT \ln K'$, where K' can be estimated through the measurement of Ca^{2+} concentrations according to the method proposed by Gebauer et al. [20]. From these calculations, it can be concluded that the smaller the counterion, either from the carbonate or the calcium sources, the greater the stabilization of the pre-nucleation species (i.e., more negative $\Delta G_{binding}$), as depicted in Figure 3a,b. This stabilizing effect is more clearly observed in the case of different anions in the calcium source

(i.e., CaX$_2$ where X = Cl$^-$, Br$^-$ or I$^-$). However, in the cases of both anions and cations, changes in ΔG$_{binding}$ were limited, and almost within error values, in comparison with reported values for other additives, such as organics, e.g., polyacrylate on CaCO$_3$ [36], citrate on calcium oxalate [37], or apatite [38].
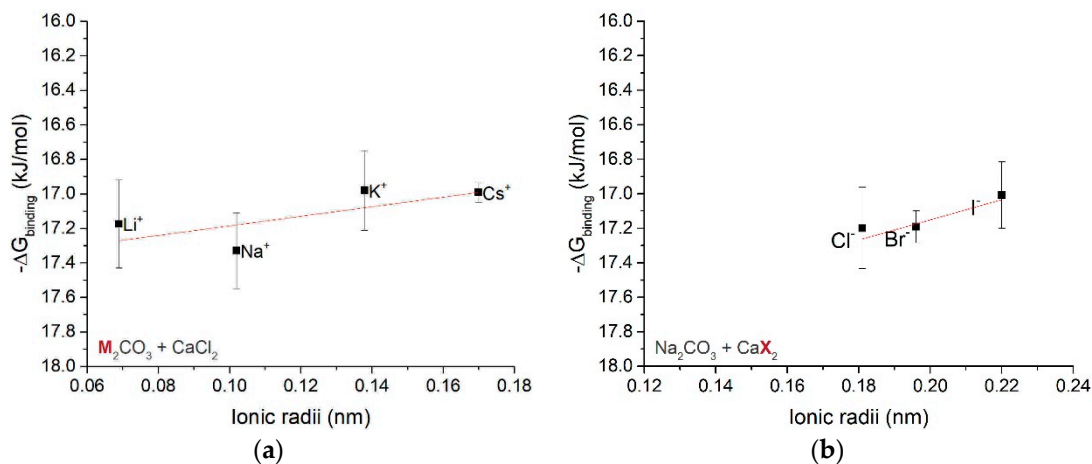
Figure 3. ΔG$_{binding}$ calculated for (**a**) different cations in the carbonate source, and (**b**) different anions in the calcium source. Errors bars show 2σ_N.

3.1.4. Particle Size and Phase Evolution

Dynamic light scattering measurements show particle sizes ranging from 20 nm to more than 1 μm (Figure 4). It is likely that particles are a mixture of all detected phases (ACC, vaterite and calcite; see phase analysis below), the smallest ones being ACC (more abundant at the early stages), and the larger ones vaterite and calcite (more abundant at later stages). It was also observed that the smaller the size of the background ion present in the solution, the broader the size distribution and the higher the amount of the smallest particles (i.e., left tail of PSD plot). This held true for both cations (especially in the case of Li$^+$, Figure 4a) and anions (especially in the case of Cl$^-$, Figure 4b). These results show that smaller precipitates were achieved using smaller background ions.
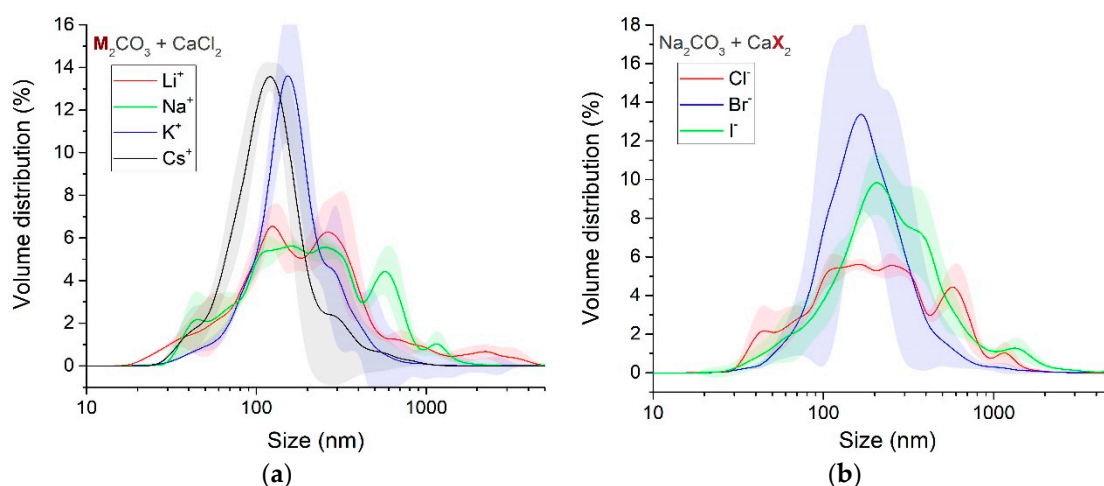
Figure 4. Particle size distribution (average of 120 consecutive measurements), expressed as volume percentage, of the precipitates during titration experiments (**a**) using different cations in the carbonate source and (**b**) using different anions in the calcium source. Shaded areas represent standard deviation from at least five titration experiments.

The morphology of the initial and final precipitates, and their mineralogy, were determined using FE-SEM images (Figure 5a–d) and X-ray diffraction analysis (Figure 5e,f). Irrespective of the type of background ions, FE-SEM observations showed spherical ACC nanoparticles from the early stages of nucleation that were consistent with the sizes detected from DLS measurements (Figure 5a). XRD analyses confirmed the amorphous nature of these early precipitates (Figure 5e). Samples collected at the very end of the titration experiments showed the presence of ~90% of vaterite and ~10% of calcite irrespective of the background electrolyte used in the titration experiment (see XRD results in Figure 5f). FE-SEM observations showed the presence of vaterite structures in close contact with calcite rhombohedra, which suggests that the latter formed after the (partial) dissolution of the former (Figure 5b). The existence of such a dissolution–precipitation process [39] was confirmed by observations of vaterite casts on (104) faces of calcite crystals (Figure S2). Interestingly, FE-SEM observations showed that vaterite structures displayed an almost perfect hexagonal plate-shaped morphology (Figure 5c). At a higher magnification, FE-SEM imaging disclosed a nanogranular structure made up of oriented vaterite nanoparticles (Figure 5d). The latter observation points to a structural development via (oriented) nanoparticle aggregation (Figure 5d), as reported by Jiang et al. [40].
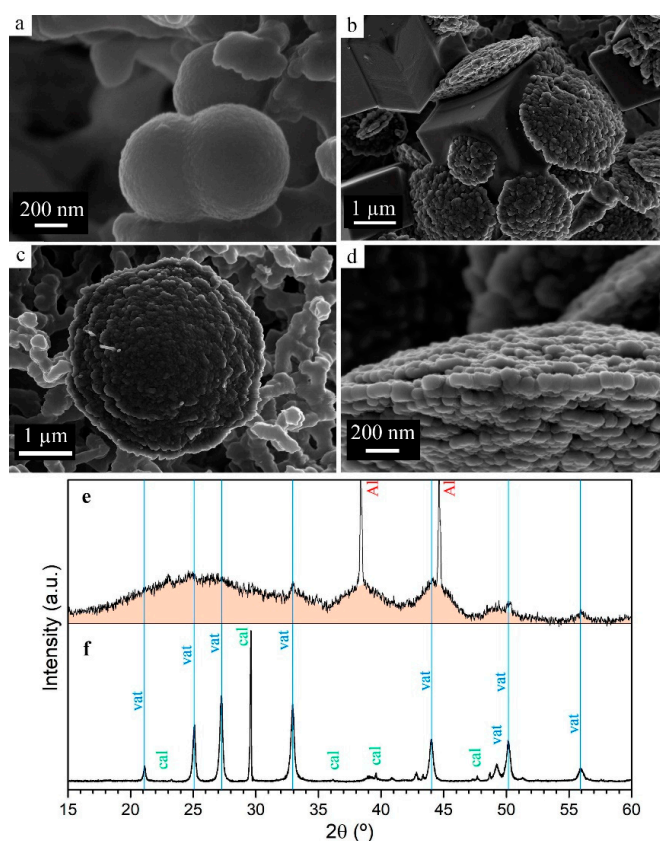
Figure 5. Representative field emission-scanning electron microscope FE-SEM images showing (**a**) spherical amorphous calcium carbonate (ACC) nanoparticles consistent in size with dynamic light scattering (DLS) measurements; (**b**) coupling of vaterite dissolution and rhombohedral calcite growth; (**c**) vaterite showing an almost perfect hexagonal plate shape; (**d**) detail of a vaterite crystal surface showing a nanogranular structure; (**e**) X-ray diffraction (XRD) analysis of precipitates obtained during titration experiments at the early stages of nucleation; and (**f**) representative diffraction pattern of samples collected at the very end of the titration experiments. Legend: cal: calcite, vat: vaterite, Al: aluminum sample holder (used as internal standard). The orange shaded area in (**e**) indicates the characteristic region of amorphous calcium carbonate (see Figure S2 for additional FE-SEM images showing the transformation of vaterite into calcite via a dissolution-precipitation process).

3.2. Type II Experiments

The main objective of this second type of experiment was to investigate the influence that background ions added as foreign electrolytes, as well as their concentration, exert on $CaCO_3$ precipitation. Titration experiments showed that in the case of the different cations (M = Li^+, Na^+, K^+ or Cs^+) in the background salt (MCl), and for the lowest ionic strength tested (IS = 0.035, [MCl] = 10 mM), a slight reduction in both the Ca^{2+}_{max} concentration (Figure 6a) and induction time (Figure 6b) were found with increasing size of background cations. However, for the highest background salt concentration tested (IS = 0.049, [MCl] = 25 mM), this trend seemed to flatten and/or slightly invert. However, note that measured values in this latter case were within error values.
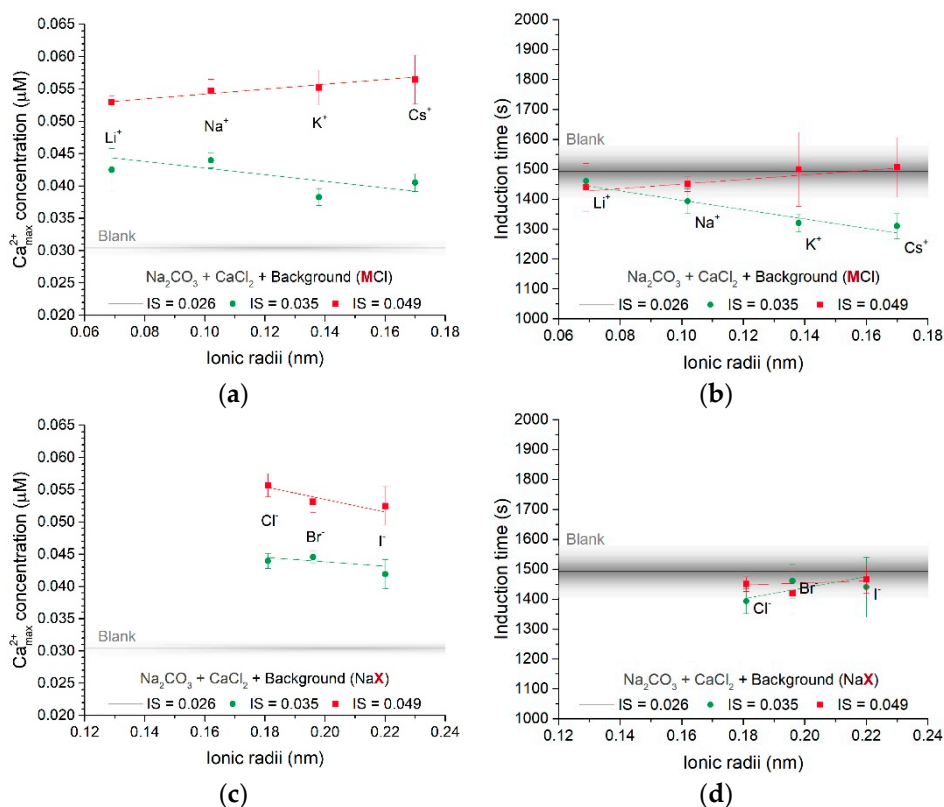
Figure 6. Maximum free Ca^{2+} concentration and elapsed time before the onset of $CaCO_3$ precipitation for type II experiments. $CaCl_2$ was used as titrant, and Na_2CO_3 as carbonate source in the reactor together with different external background salts (**a,b**) using different chloride salts, (**c,d**) using different sodium salts. Two different background electrolyte concentrations (10 and 25 mM) were used, increasing the ionic strength (IS) to 0.035 (green lines) and 0.049 (red lines), respectively. Errors bars show $2\sigma_N$. The blank black line and grey band show the average value and $2\sigma_N$, respectively, from titration experiments without any external background salt.

In the case of the different anions (X = Cl^-, Br^- or I^-) in the background salt (NaX), an apparent slight reduction in Ca^{2+}_{max} with increasing size of the background anions, and an increase in Ca^{2+}_{max} with increasing background salt concentrations were observed (Figure 6c). Induction times were within error values and similar in all cases (Figure 6d).

4. Discussion

Background electrolytes have been shown to modify both the growth and the dissolution of many minerals, e.g., gypsum, calcite, barite, whewellite, among others [21,22,24,25,41–50]. Ions at the mineral-solution interface are continuously attaching to and detaching from step edges and,

consequently, mineral dissolution or growth kinetics depend on energy barriers involving these ions [51]. However, nucleation is a precondition for mineral growth, and is interpreted as an energetic event in which a system tends towards a reduction in its total free energy once activation energy barriers are overcome [52,53]. In this energetic scenario, several different interactions have to be considered (i.e., water-water, ion-water, and ion-ion interactions) [54], which will affect both the pre-nucleation and nucleation regimes.

4.1. Ion-Water Interactions

As a result of their charge, ions in solution promote the development of two distinct hydration regions around themselves: one closer to the ion, in which water is tightly bound and electrostricted as a hydration (inner) shell; and (outer shell) water that is under the influence of the electric field of the ions within the bulk water [27]. Ions interact with water molecules around them, forming a "cavity in the water" of radius $r + \Delta r$ (i.e., an ion plus its hydration shell), which allows them to interact with the bulk water as if it were uncharged due to charge dispersion and dipole-induced forces between water molecules and the ion [55]. The mobility of water molecules in the vicinity of ions has been well-studied through numerous experimental and theoretical investigations [56]. This water mobility controls the diffusion of ions in aqueous solutions. Frequently, it has been presented as the ratio between the residence time of a water molecule in the solvation shell of the ion and in pure water (i.e., τ_i/τ_0) [57]. The latter depends on the competition between the tendency of an ion to orient water molecules in its solvation shell and the opposition of water to disrupt its hydrogen-bonded network [58]. Additionally, Samoĭlov [59] pointed out that residence times are also due to differences in the activation energies (ΔE_i) between removing a water molecule from the ion solvation shell (E_i), and the activation energy required for transferring a water molecule from the first to the next coordination shell of another water molecule (E_0). Therefore, the aforementioned parameters allow us to define ions as positively or negatively hydrated, according to a retarded (i.e., $\tau_i > \tau_0$; $\Delta E_i > 0$) or an increased ($\tau_i < \tau_0$; $\Delta E_i < 0$) mobility of water from the solvation shell, respectively [30].

Small ions present a high charge density (i.e., high ionic potential), that results in strong hydration due to a closer approximation between the point charge of the ion and the point charge of the opposite charge in the water molecules [54]. This results in a higher activation energy needed to remove a water molecule from the ion solvation shell (E_i) and a longer residence time (τ_i) of a water molecule in the ion solvation shell. Therefore, hydration effects in aqueous solutions are highly dependent on the size and charge of the ions present. This inevitably will profoundly influence both the dissolution and growth of a mineral, as the characteristics of the aqueous solutions from which growth or dissolution occurs change depending on the ions in the solution.

4.2. Calcium Carbonate Pre-Nucleation Clusters

Gebauer et al. have reported on the existence of stable calcium carbonate pre-nucleation clusters (PNC) based on ion potential measurements in combination with analytical ultracentrifugation results [60]. This has also been confirmed by cryogenic transmission electron microscopy [60] and, additionally, through atomistic computational simulations [18]. The size of calcium carbonate PNC has been estimated to be below 2 nm; however, discrepancies on the exact size value exist due to the effect of surrounding hydration layers. Such hydration layers could be influenced by the electrostatic environment related to the nature of the background ionic species present in the solution.

Hydration of both Ca^{2+} and CO_3^{2-} ions, and/or PNC, which are considered solute species [20,52], in the presence of background ions will be controlled by the dynamics of water molecules in such solutions (E_{BCKG_0}), apart from the potential mineral structure-building ions and/or PNC interactions with solvent molecules (E_{BCKG_i}). In the presence of background ions, water–water interactions would be different with respect to pure water, due to the electrostatic environment related to background ions present in the solution. The stronger the background ion–water interactions (X^--H_2O and M^+-H_2O) resulting from higher charge density and lower ionic size, the higher the

activation energy barrier of expelling water from the solvation shells of background ions [24,61,62]. Consequently, the more structured the water network, the lower the activation energy required to break water–water interactions in the presence of background ions (E_{BCKG_0}). Restricted water movement at the PNC-solution interface (i.e., Li^+ or Cl^-) would hinder phase separation, because desolvation would be the rate-limiting step for nucleation [10,61].

Also, the presence of background ions (M^+ and X^-) influences the required energy to strip off a water molecule from the solvation shell of a structure-forming ion (such as Ca^{2+} and CO_3^{2-}) and/or from PNC solute species. At low ionic strength, similar to our working conditions, the average distance between ions building the crystal and background counterions ($Ca^{2+}//X^-$ and/or $CO_3^{2-}//M^+$) is smaller than between ions building the crystal and background ions with the same charge sign [63]. Background ions with a different charge sign (counterions) with respect to Ca^{2+} or CO_3^{2-} ions reduce the potential energy of water molecules in the Ca^{2+} or CO_3^{2-} solvation shells, as a result of attractive interactions between the partial charge of the water dipole and the oppositely charged electric field of the counterions [24,64,65]. The latter results in stabilization and, therefore, increasing residence times of these water molecules (τ_{BCKG_i}) in the Ca^{2+} or CO_3^{2-} solvation shells.

The stabilization of water molecules both surrounding and incorporated within PNC, by a strengthening of the electric field emanating from background ions, could decrease the dynamics of the clusters' equilibrium and stabilize pre-nucleation species. However, their dehydration and subsequent transformation into solid species would be also hampered. According to our results, the smaller the size of the background ion, and therefore the stronger its interaction with water, the larger the overall reduction in ΔG_{PNC}, resulting in a stabilization of PNC and a less favorable calcium carbonate precipitation. The latter is in agreement with the higher free Ca^{2+} concentration reached, and the resulting retardation of the onset of nucleation.

In summary, the solvation shell stability of either Ca^{2+}, CO_3^{2-}, ion pairs and/or PNC will depend, among other variables, on the characteristics of the background ions present in the solution. According to our experimental results, background ions induce stabilization of PNC, as deduced from the overall values of $\Delta G_{binding}$ (see Figure 3), according to the following trend $Li^+ > Na^+ > K^+ \geq Cs^+$ for the cations, and $Cl^- > Br^- > I^-$ for the anions (i.e., higher stabilization is achieved with decreasing ionic radius). More negative $\Delta G_{binding}$ values (such as in the case of Li^+ as a carbonate source or Cl^- as a calcium source), would limit dehydration kinetics of PNC by increasing the residence time of water molecules entering into their structure. Thus, longer induction times and higher supersaturation values would be required before the onset of nucleation occurs. The higher supersaturation values required for the onset of nucleation would lead to lower particle sizes [10], which is in agreement with our DLS experimental results (as seen in the left tails in the PSD plots shown in Figure 4).

4.3. Effects on ACC Solubility and Polymorph Selection

Two different ACC "polyamorphs" have been reported in the literature, ACC I and ACC II [20], with different solubilities attributed to their proto-calcite and proto-vaterite structure, respectively. However, we have not found any clear relationship between observed lower or higher solubilities determined following titration experiments and the final polymorph selection. Actually, calcite-vaterite ratios were similar, within error, for all the different experimental precipitation runs. In our experiments, it is not clear whether or not a specific ACC proto-structure determines the phase selection. In all cases, the first phase formed after ACC (irrespective of ACC solubility) is vaterite, that during a dissolution–precipitation process transforms into calcite, although such a replacement is incomplete within the time-span of our titration experiments.

An alternative explanation for the existence of ACC nanoparticles with a higher solubility (i.e., runs including Li^+ or Cl^-, Figure 2) might be related to particle size effects. Zou et al. [34] have shown that there is a clear relationship between ACC particle size and solubility, which increases with decreasing ACC particle diameter (for particles with diameter <200 nm). This is fully consistent with our DLS measurements (Figure 4) showing that the left-tails (i.e., smallest particle size) of PSD

plots expand to smaller sizes in the presence of Li$^+$, as well as for Cl$^-$. It should be also considered that another explanation for the measured solubility could be related to variations in the water content of ACC. Rodriguez-Navarro et al. have shown that there is a linear correlation between water content in ACC and solubility (i.e., lower solubility in anhydrous ACC and increased solubility as the water content in ACC increases) [33]. However, in all cases, the dissolution of ACC particles resulted in a solution with a sufficiently high supersaturation with respect to vaterite, as to enable its precipitation (following Ostwald's step rule) [10].

4.4. Influence of Background Electrolyte Concentration

Our results show that in type II experiments, differences in both induction time and Ca$^{2+}_{max}$ concentration for CaCO$_3$ nucleation diminished with increasing concentration of background electrolytes, and therefore the solution ionic strength, through the addition of different 1:1 salts. This suggests that at low ionic strength (i.e., low background electrolyte concentration), the electrostatic environment created by background ions controls ion–water interactions, while also depending substantially on the nature of the background electrolyte [26,54]. With the addition of background electrolytes with smaller ionic sizes, Ca^{2+}, CO$_3^{2-}$, ion pairs and/or PNCs will be stabilized, as stated above, and subsequently the time required for nucleation will be higher (see Figure 6).

However, at higher background electrolyte concentrations (and higher ionic strengths), the destabilizing effect, induced by the presence of like-charge ions on PNC hydration water, will become increasingly important, due to the reduced average distance between ionic species. This is because of like-charge ions in the solution, and the effect of background ions on the PNC hydration, which will stop controlling ion–water interactions (τ_{BCKG_i}) [63,65]. However, background electrolytes may still influence bulk solvent structure dynamics (τ_{BCKG_0}). The stronger the interaction between background ions and water, the weaker the hydration of structure-forming ions (or PNC). Therefore, clustering and dehydration would be favored, enhancing the nucleation of a solid phase. However, no reduction in the induction times for nucleation was observed when an enhancement of CaCO$_3$ precipitation with increasing IS should be expected. The latter could be attributed to our experimental design, due to the impossibility to fix both IS and pH. When increasing the background electrolyte concentration, the pH slightly decreased, which, according to Gebauer et al. [20], results in an increase in both the induction time and Ca$^{2+}_{max}$ for CaCO$_3$ precipitation that may counteract the theoretically expected decrease in nucleation time.

Finally, we stress that the observed background electrolyte effects should not be constrained to the nucleation and growth of calcium carbonate; they also should play a role in the dissolution of this phase. This is consistent with differences in both dissolution rates, measured from in situ flow-through calcite dissolution experiments using atomic force microscopy (AFM) [22,49,66], and atypical surface morphological features development, as in the presence of NH$_4$Cl background ions, which lead to spicule formation on {104} calcite surfaces [67].

5. Conclusions

First, it should be considered that water molecules in the solvation shell of a solute ion are stabilized by the presence of background counterions in the solution [65,68]. The increased affinity of water molecules for solute ions hampers precipitation in the case of strongly hydrated background ions (e.g., Li$^+$ and Cl$^-$). This is related to the structuring effect of water molecules when they are ordered around strongly hydrated ions and/or clusters. If the hydration shells of ions and/or clusters are stabilized due to the presence of background salts, the overall precipitation process would be hampered.

Our results suggest that the ACC solubility differences found in experiments with specific background ions (e.g., in the case of Li$^+$ in the carbonate source or Cl$^-$ in the calcium source) might not be related to a specific ACC protostructure, but rather to the particle size of ACC formed at the very early stages of precipitation and/or the degree of hydration of ACC. Such solubility (and stability)

differences are related to the ionic radius of background electrolyte ions. Due to the presence of strongly hydrated background electrolytes, the stabilization of pre-nucleation species results in higher supersaturation values and longer induction times before the onset of nucleation occurs. The latter is also in agreement with the observed lower particle sizes.

These results have important implications not only for a better understanding of non-classical crystallization of calcium carbonate in laboratory experiments, but also in natural environments. It should be pointed out that a comparison between calcium carbonate precipitation experiments by different researchers may not be straightforward because of the use of different reactants and IS. We also suggest that stabilization of PNC by specific background electrolytes can be selectively used to favor or hinder the precipitation or transport in solution of calcium carbonate in industrial and pharmaceutical processes.

Supplementary Materials: The following are available online at www.mdpi.com/2075-163X/7/7/126/s1, Figure S1: (a) Enthalpy of hydration vs. ionic radii and (b) Standard molar Gibbs energy of hydration of an ion vs. ionic radii. Note the quasilinear relationship between both variables with decreasing ionic radii; Figure S2: FESEM images of vaterite to calcite transition from the same titration run as seen in Figure 5b showing (a) vaterite attached to calcite. The development of growth steps is observed on the calcite surface; and (b) calcite crystals with vaterite casts.

Author Contributions: Encarnacion Ruiz-Agudo conceived and designed the experiments; Alejandro Burgos-Cara performed the experiments; Alejandro Burgos-Cara and Christine V. Putnis analyzed the data; Carlos Rodriguez-Navarro contributed analysis tools; Alejandro Burgos-Cara and Carlos Rodriguez-Navarro wrote the paper, with contributions from all authors.

Conflicts of Interest: The authors declare no conflict of interest.

References

1. Gower, L.B. Biomimetic model systems for investigating the amorphous precursor pathway and its role in biomineralization. *Chem. Rev.* **2008**, *108*, 4551–4627. [CrossRef] [PubMed]
2. Cam, N.; Georgelin, T.; Jaber, M.; Lambert, J.F.; Benzerara, K. In vitro synthesis of amorphous Mg-, Ca-, Sr- and Ba-carbonates: What do we learn about intracellular calcification by cyanobacteria? *Geochim. Cosmochim. Acta* **2015**, *161*, 36–49. [CrossRef]
3. Zhong, C.; Chu, C.C. Acid polysaccharide-induced amorphous calcium carbonate (ACC) films: Colloidal nanoparticle self-organization process. *Langmuir* **2009**, *25*, 3045–3049. [CrossRef] [PubMed]
4. Tobler, D.J.; Blanco, J.D.R.; Dideriksen, K.; Sand, K.K.; Bovet, N.; Benning, L.G.; Stipp, S.L.S. The effect of aspartic acid and glycine on amorphous calcium carbonate (ACC) structure, stability and crystallization. *Proced. Earth Planet. Sci.* **2014**, *10*, 143–148. [CrossRef]
5. Bentov, S.; Weil, S.; Glazer, L.; Sagi, A.; Berman, A. Stabilization of amorphous calcium carbonate by phosphate rich organic matrix proteins and by single phosphoamino acids. *J. Struct. Biol.* **2010**, *171*, 207–215. [CrossRef] [PubMed]
6. De Yoreo, J.J.; Dove, P.M. Shaping crystals with biomolecules. *Science* **2004**, *306*, 1301–1302. [CrossRef] [PubMed]
7. Zeng, J.; Yin, Z.; Chen, Q. Effect of tetracarbon additives on gibbsite precipitation from seeded sodium aluminate liquor. *J. Cent. South Univ. Technol.* **2008**, *15*, 622–626. [CrossRef]
8. Orshesh, Z.; Hesaraki, S.; Khanlarkhani, A. Blooming gelatin: An individual additive for enhancing nanoapatite precipitation, physical properties, and osteoblastic responses of nanostructured macroporous calcium phosphate bone cements. *Int. J. Nanomed.* **2017**, *12*, 745–758. [CrossRef] [PubMed]

9. Wolf, S.E.; Böhm, C.F.; Harris, J.; Demmert, B.; Jacob, D.E.; Mondeshki, M.; Ruiz-Agudo, E.; Rodríguez-Navarro, C. Nonclassical crystallization in vivo et in vitro (I): Process-structure-property relationships of nanogranular biominerals. *J. Struct. Biol.* **2016**, *196*, 244–259. [CrossRef] [PubMed]

10. Rodríguez-Navarro, C.; Ruiz-Agudo, E.; Harris, J.; Wolf, S.E. Nonclassical crystallization in vivo et in vitro (II): Nanogranular features in biomimetic minerals disclose a general colloid-mediated crystal growth mechanism. *J. Struct. Biol.* **2016**, *196*, 260–287. [CrossRef] [PubMed]

11. Lowenstam, H.A.; Weiner, S. *On Biomineralization*; Oxford University Press: Oxford, UK, 1989.

12. Gago-Duport, L.; Briones, M.J.I.; Rodríguez, J.B.; Covelo, B. Amorphous calcium carbonate biomineralization in the earthworm's calciferous gland: Pathways to the formation of crystalline phases. *J. Struct. Biol.* **2008**, *162*, 422–435. [CrossRef] [PubMed]

13. Loste, E.; Wilson, R.M.; Seshadri, R.; Meldrum, F.C. The role of magnesium in stabilising amorphous calcium carbonate and controlling calcite morphologies. *J. Cryst. Growth* **2003**, *254*, 206–218. [CrossRef]

14. Gonzalez-Munoz, M.T.; Ben Chekroun, K.; Ben Aboud, A.; Arias, J.M.; Rodriguez-Gallego, M. Bacterially induced Mg-calcite formation: Role of Mg^{2+} in development of crystal morphology. *J. Sediment. Res.* **2000**, *70*, 559–564. [CrossRef]

15. Davis, K.J. The Role of Mg^{2+} as an Impurity in Calcite Growth. *Science* **2000**, *290*, 1134–1137. [CrossRef] [PubMed]

16. Zhang, Y.; Dawe, R.A. Influence of Mg^{2+} on the kinetics of calcite precipitation and calcite crystal morphology. *Chem. Geol.* **2000**, *163*, 129–138. [CrossRef]

17. Berg, J.K.; Jordan, T.; Binder, Y.; Börner, H.G.; Gebauer, D. Mg^{2+} Tunes the Wettability of Liquid Precursors of $CaCO_3$: Toward Controlling Mineralization Sites in Hybrid Materials. *J. Am. Chem. Soc.* **2013**, *135*, 12512–12515. [CrossRef] [PubMed]

18. Demichelis, R.; Raiteri, P.; Gale, J.D. Structure of hydrated calcium carbonates: A first-principles study. *J. Cryst. Growth* **2013**. [CrossRef]

19. Demichelis, R.; Raiteri, P.; Gale, J.D.; Quigley, D.; Gebauer, D. Stable prenucleation mineral clusters are liquid-like ionic polymers. *Nat. Commun.* **2011**, *2*, 590. [CrossRef] [PubMed]

20. Gebauer, D.; Volkel, A.; Colfen, H. Stable prenucleation calcium carbonate clusters. *Science* **2008**, *322*, 1819–1822. [CrossRef] [PubMed]

21. Burgos-Cara, A.; Putnis, C.V.; Rodriguez-Navarro, C.; Ruiz-Agudo, E. Hydration effects on gypsum dissolution revealed by in situ nanoscale atomic force microscopy observations. *Geochim. Cosmochim. Acta* **2016**, *179*, 110–122. [CrossRef]

22. Ruiz-Agudo, E.; Kowacz, M.; Putnis, C.V.; Putnis, A. The role of background electrolytes on the kinetics and mechanism of calcite dissolution. *Geochim. Cosmochim. Acta* **2010**, *74*, 1256–1267. [CrossRef]

23. Ruiz-Agudo, E.; Putnis, C.V.; Wang, L.; Putnis, A. Specific effects of background electrolytes on the kinetics of step propagation during calcite growth. *Geochim. Cosmochim. Acta* **2011**, *75*, 3803–3814. [CrossRef]

24. Kowacz, M.; Putnis, A. The effect of specific background electrolytes on water structure and solute hydration: Consequences for crystal dissolution and growth. *Geochim. Cosmochim. Acta* **2008**, *72*, 4476–4487. [CrossRef]

25. Ruiz-Agudo, E.; Urosevic, M.; Putnis, C.V.; Rodríguez-Navarro, C.; Cardell, C.; Putnis, A. Ion-specific effects on the kinetics of mineral dissolution. *Chem. Geol.* **2011**, *281*, 364–371. [CrossRef]

26. Collins, K.D.; Neilson, G.W.; Enderby, J.E. Ions in water: Characterizing the forces that control chemical processes and biological structure. *Biophys. Chem.* **2007**, *128*, 95–104. [CrossRef] [PubMed]

27. Marcus, Y. Thermodynamics of solvation of ions. Part 5.—Gibbs free energy of hydration at 298.15 K. *J. Chem. Soc. Faraday Trans.* **1991**, *87*, 2995–2999. [CrossRef]

28. Saharay, M.; Yazaydin, A.O.; Kirkpatrick, R.J. Dehydration-induced amorphous phases of calcium carbonate. *J. Phys. Chem. B* **2013**, *117*, 3328–3336. [CrossRef] [PubMed]

29. Saharay, M.; James Kirkpatrick, R. Onset of orientational order in amorphous calcium carbonate (ACC) upon dehydration. *Chem. Phys. Lett.* **2014**, *591*, 287–291. [CrossRef]

30. Kowacz, M.; Prieto, M.; Putnis, A. Kinetics of crystal nucleation in ionic solutions: Electrostatics and hydration forces. *Geochim. Cosmochim. Acta* **2010**, *74*, 469–481. [CrossRef]

31. Kielland, J. Individual activity coefficients of ions in aqueous solutions. *J. Am. Chem. Soc.* **1937**, *59*, 1675–1678. [CrossRef]

32. Zhuo, K.; Dong, W.; Wang, W.; Wang, J. Activity coefficients of individual ions in aqueous solutions of sodium halides at 298.15 K. *Fluid Phase Equilib.* **2008**, *274*, 80–84. [CrossRef]

33. Rodriguez-Navarro, C.; Kudlacz, K.; Cizer, O.; Ruiz-Agudo, E.; Kudłacz, K.; Cizer, Ö.; Ruiz-Agudo, E.; Kudlacz, K.; Cizer, O.; Ruiz-Agudo, E. Formation of amorphous calcium carbonate and its transformation into mesostructured calcite. *CrystEngComm* **2015**, *17*, 58–72. [CrossRef]

34. Zou, Z.; Bertinetti, L.; Politi, Y.; Jensen, A.C.S.; Weiner, S.; Addadi, L.; Fratzl, P.; Habraken, W.J.E.M. Opposite particle size effect on amorphous calcium carbonate crystallization in water and during heating in air. *Chem. Mater.* **2015**, *27*, 4237–4246. [CrossRef]

35. Parkhurst, D.L.; Appelo, C.A.J. *Description of Input and Examples for PHREEQC Version 3–A Computer Program for Speciation, Batch-Reaction, One-Dimensional Transport, and Inverse Geochemical Calculations*; U.S. Geological Survey: Reston, VA, USA, 2013.

36. Verch, A.; Gebauer, D.; Antonietti, M.; Cölfen, H. How to control the scaling of $CaCO_3$: A "fingerprinting technique" to classify additives. *Phys. Chem. Chem. Phys.* **2011**, *13*, 16811–16820. [CrossRef] [PubMed]

37. Qiu, S.R.; Wierzbicki, A.; Salter, E.A.; Zepeda, S.; Orme, C.A.; Hoyer, J.R.; Nancollas, G.H.; Cody, A.M.; De Yoreo, J.J. Modulation of calcium oxalate monohydrate crystallization by citrate through selective binding to atomic steps. *J. Am. Chem. Soc.* **2005**, *127*, 9036–9044. [CrossRef] [PubMed]

38. Hu, Y.-Y.; Rawal, A.; Schmidt-Rohr, K. Strongly bound citrate stabilizes the apatite nanocrystals in bone. *Proc. Natl. Acad. Sci. USA* **2010**, *107*, 22425–22429. [CrossRef] [PubMed]

39. Rodriguez-Blanco, J.D.; Shaw, S.; Benning, L.G. The kinetics and mechanisms of amorphous calcium carbonate (ACC) crystallization to calcite, via vaterite. *Nanoscale* **2011**, *3*, 265–271. [CrossRef] [PubMed]

40. Jiang, W.; Pacella, M.S.; Athanasiadou, D.; Nelea, V.; Vali, H.; Hazen, R.M.; Gray, J.J.; McKee, M.D. Chiral acidic amino acids induce chiral hierarchical structure in calcium carbonate. *Nat. Commun.* **2017**, *8*, 15066. [CrossRef] [PubMed]

41. Bosbach, D.; Junta-Rosso, J.L.; Becker, U.; Hochella, M.F. Gypsum growth in the presence of background electrolytes studied by scanning force microscopy. *Geochim. Cosmochim. Acta* **1996**, *60*, 3295–3304. [CrossRef]

42. Wolthers, M.; Nehrke, G.; Gustafsson, J.P.; Van Cappellen, P. Calcite growth kinetics: Modeling the effect of solution stoichiometry. *Geochim. Cosmochim. Acta* **2012**, *77*, 121–134. [CrossRef]

43. Weaver, M.L.; Qiu, S.R.; Hoyer, J.R.; Casey, W.H.; Nancollas, G.H.; De Yoreo, J.J. Inhibition of calcium oxalate monohydrate growth by citrate and the effect of the background electrolyte. *J. Cryst. Growth* **2007**, *306*, 135–145. [CrossRef]

44. Putnis, C.V.; Ruiz-Agudo, E. The mineral-water interface: Where minerals react with the environment. *Elements* **2013**, *9*, 177–182. [CrossRef]

45. Ruiz-Agudo, E.; Putnis, C.V.; Rodriguez-Navarro, C. Reactions between minerals and aqueous solutions. In *Mineral Reaction Kinetics: Microstructures, Textures, Chemical and Isotopic Signatures*; Mineralogical Society of Great Britain & Ireland: Middlesex, UK, 2017; Volume 16, pp. 419–467.

46. Dove, P.M.; Czank, C.A. Crystal chemical controls on the dissolution kinetics of the isostructural sulfates: Celestite, anglesite, and barite. *Geochim. Cosmochim. Acta* **1995**, *59*, 1907–1915. [CrossRef]

47. Pokrovsky, O.S.; Schott, J. Iron colloids/organic matter associated transport of major and trace elements in small boreal rivers and their estuaries (NW Russia). *Chem. Geol.* **2002**, *190*, 141–179. [CrossRef]

48. Kowacz, M.; Groves, P.; Esperança, J.M.S.S.; Rebelo, L.P.N. On the use of ionic liquids to tune crystallization. *Cryst. Growth Des.* **2011**, *11*, 684–691. [CrossRef]

49. Ruiz-Agudo, E.; Putnis, C.V. Direct observations of mineral fluid reactions using atomic force microscopy: The specific example of calcite. *Mineral. Mag.* **2012**, *76*, 227–253. [CrossRef]

50. Aoba, T. The effect of fluoride on apatite structure and growth. *Crit. Rev. Oral Biol. Med.* **1997**, *8*, 136–153. [CrossRef] [PubMed]

51. DeYoreo, J.J.; Vekilov, P.G. Principles of crystal nucleation and growth. *Rev. Mineral. Geochem.* **2003**, *54*, 57–93. [CrossRef]

52. Gebauer, D.; Kellermeier, M.; Gale, J.D.; Bergström, L.; Cölfen, H. Pre-nucleation clusters as solute precursors in crystallisation. *Chem. Soc. Rev.* **2014**, *43*, 2348–2371. [CrossRef] [PubMed]

53. Sear, R.P. Nucleation: Theory and applications to protein solutions and colloidal suspensions. *J. Phys. Condens. Matter* **2007**, *19*, 33101. [CrossRef]

54. Collins, K.D. Charge density-dependent strength of hydration and biological structure. *Biophys. J.* **1997**, *72*, 65–76. [CrossRef]

55. Collins, K.D. Ion hydration: Implications for cellular function, polyelectrolytes, and protein crystallization. *Biophys. Chem.* **2006**, *119*, 271–281. [CrossRef] [PubMed]

56. Marcus, Y. Effect of ions on the structure of water: Structure making and breaking. *Chem. Rev.* **2009**, *109*, 1346–1370. [CrossRef] [PubMed]

57. Marcus, Y. *Ions in Water and Biophysical Implications*; Springer: Dordrecht, The Netherlands, 2012; Volume 53.

58. Hribar, B.; Southall, N.T.; Vlachy, V.; Dill, K.A. How ions affect the structure of water. *J. Am. Chem. Soc.* **2002**, *124*, 12302–12311. [CrossRef] [PubMed]

59. Samoĭlov, O.I. *Structure of Aqueous Electrolyte Solutions and the Hydration of Ions*; Consultants Bureau: London, UK, 1965.

60. Pouget, E.M.; Bomans, P.H.H.; Goos, J.A.C.M.; Frederik, P.M.; de With, G.; Sommerdijk, N.A.J.M. The initial stages of template-controlled $CaCO_3$ formation revealed by cryo-TEM. *Science* **2009**, *323*, 1455–1458. [CrossRef] [PubMed]

61. Dorvee, J.R.; Veis, A. Water in the formation of biogenic minerals: Peeling away the hydration layers. *J. Struct. Biol.* **2013**, *183*, 278–303. [CrossRef] [PubMed]

62. Malenkov, G.G.; Samoĭlov, O.I. Electrostatic interaction and coordination of molecules in water. *J. Struct. Chem.* **1965**, *6*, 6–10. [CrossRef]

63. Kinoshita, M.; Harano, Y. Potential of mean force between solute atoms in salt solution: Effects due to salt species and relevance to conformational transition of biomolecules. *Bull. Chem. Soc. Jpn.* **2005**, *78*, 1431–1441. [CrossRef]

64. Samoĭlov, O.I. The theory of the salting out in aqueous solutions-II. Dependence of dehydration and hydration on the initial degree of hydration of a cation undergoing salting out. *J. Struct. Chem.* **1967**, *7*, 177–180. [CrossRef]

65. Samoĭlov, O.I. Theory of salting out from aqueous solutions-III. Dependence of salting out on characteristics of ions of salting-out agent. *J. Struct. Chem.* **1971**, *11*, 929–931. [CrossRef]

66. Buhmann, D.; Dreybrodt, W. Calcite dissolution kinetics in the system H_2O-CO_2-$CaCO_3$ with participation of foreign ions. *Chem. Geol.* **1987**, *64*, 89–102. [CrossRef]

67. Long, X.; Meng, R.; Wu, W.; Ma, Y.; Yang, D.; Qi, L. Calcite microneedle arrays produced by inorganic ion-assisted anisotropic dissolution of bulk calcite crystal. *Chem.-A Eur. J.* **2014**, *20*, 4264–4272. [CrossRef] [PubMed]

68. Samoĭlov, O.I. The theory of salting out from aqueous solutions-I. General problems. *J. Struct. Chem.* **1967**, *7*, 12–19. [CrossRef]